The International Archives of the Photogrammetry, Remote Sensing and Spatial Information Sciences, Volume XLVIII-2/W3-2023
ISPRS Intl. Workshop "Photogrammetric and computer vision techniques for environmental and infraStructure monitoring, Biometrics and Biomedicine"
PSBB23, 24–26 April 2023, Moscow, Russia

NON-CONVEX HYBRID TOTAL VARIATION FOR RESTORING MEDICAL IMAGE CORRUPTED BY POISSON NOISE

Thi Thu Thao Tran[1], Cong Thang Pham[2 *], Hoai Phuong Dang[2], Andrey Kopylov[3], Van Ha Mai[2], The Xuan Ly Nguyen[2]

[1]The University of Danang-University of Economics, 71 Ngu Hanh Son, Danang, Viet Nam
thaotran@due.udn.vn

[2]The University of Danang-University of Science and Technology, 54 Nguyen Luong Bang, Danang, Viet Nam
(pcthang, dhphuong, mvha, ntxly)@dut.udn.vn

[3] Tula State University, 92 Lenin Ave., Tula, Russia And.Kopylov@gmail.com

Commission II, WG II/8

KEY WORDS: Adaptive model, Medical image denoising, Mixed noise, Total variation, Laplacian regularizer, Primal-dual.

ABSTRACT:

In this work, we proposed the hybrid non-convex regularizers for Poisson noise removal on medical images. The model is built by a combination of non-convex total variation and non-convex fractional total variation. The proposed model allows for avoiding the annoying staircase artifacts and obtaining the reconstruction results with sharp and neat edges during the noise removal process. For handling the minimization problem, we employ the alternating minimization method associated with the iteratively reweighted l_1 algorithm. Numerical experiments illustrate the efficiency of the proposed model and corresponding algorithm.

1. INTRODUCTION

Image is often contaminated by noise during the generation, transmission, and acquisition processes. In this work, we mainly focus on the removal of Poisson noise in positron emission tomography (PET) such as computerized tomography (CT) and magnetic resonance imaging (MRI), etc. In these systems, images are generated by photon counting which follows the Poisson process. Hence, noise present in images also follows Poisson distribution (Hasinoff, 2014, Pham, 2023).

There are many methods proposed for suppressing Poisson noise. Among them, methods that use the norm of total variation (TV) as a regularization are commonly adopted (Le et al., 2007). Under the TV framework, the TV-based Poisson noise removal model has the following form (Le et al., 2007):

$$\mathbf{X}^* = \arg\min_{\mathbf{X}} \left(\int_{\mathcal{B}} |\nabla \mathbf{X}|\, dx + \beta \int_{\Omega} (\mathbf{X} - \mathbf{Y}\log \mathbf{X}) dx, \right), \tag{1}$$

where $\mathbf{Y}$ is the observed image,
$\mathcal{B} \subset \mathcal{R}^2$,
$\mathbf{X}$ is positive over $\mathcal{B}$,
β is positive regularization parameter.

As is well known, the TV regularization framework allows us to obtain denoising results with sharp edges. However, TV-based model (1) often leads to undesired staircase effects and smooth out image textures (Liu et al. 2013, Kayyar et al. 2018, Pham, 2021a). To overcome the issue, some higher-order TV models were developed for image denoising with edge-preserving (Kayyar et al. 2018, Ma et al. 2020, Pham, 2021b).

One successful approach is fractional order TV, which is widely applied in image restoration. Authors in (Chowdhury et al., 2020) proposed the fractional-order TV model (FTV) for Poisson image denoising as follows:

$$\mathbf{X}^* = \arg\min_{\mathbf{X}} \int_{\mathcal{B}} |\nabla^{\alpha} \mathbf{X}|\, dx + \beta \int_{\mathcal{B}} (\mathbf{X} - \mathbf{Y}\log \mathbf{X}) dx, \tag{2}$$

where β is positive regularization parameter,
$\nabla^{\alpha} u$ represents for fractional-order total variation.

Unfornatively, methods based on the fractional-order TV may cause image blurring. Hence, authors (Tran, 2021) proposed model combining the advantages of two above total variation regularization models for Poisson noise removal as follows (named by hybrid total variation regularization model, HTVRM):

$$\begin{aligned} \mathbf{X}^* = \arg\min_{X} \Big(& \gamma_1 \int_{\mathcal{B}} |\nabla \mathbf{X}|\, dx \\ & + \gamma_2 \int_{\mathcal{B}} |\nabla^{\alpha} \mathbf{X}|\, dx + \beta \int_{\Omega} (\mathbf{X} - \mathbf{Y}\log \mathbf{X}) dx, \Big), \end{aligned} \tag{3}$$

where γ_1, γ_2 and β are positive parameters.

However, the above-mentioned model with convex regularizers suffers from certain limits, such as overly blurred contours and edges, or residual noise. To improve the edge-preserving ability, non-convex regularization is proposed with better sparsity and robustness on the basis of guaranteeing a better solution than a convex one (Lian W. et al., 2023). Additionally, non-convex regularization models can obtains high quality image with sharp and neat edges (Nikolova, 2010, Tang, 2019)

* Corresponding author: pcthang@dut.udn.vn

Motivated by the previous works, we focus on the model (3) and propose the non-convex hybrid total variation model for Poissonian image denoising. The main contributions of this work are the following: we propose a novel model for Poissonian Image denoising based on the combination of non-convex first-order TV and non-convex fractional order TV. The proposed model allows for avoiding annoying staircase artifacts and keeps sharp contours during the noise removal process. Furthermore, we combine the iteratively reweighted l_1 algorithm and extended alternating minimization method to handle the corresponding minimization problem. Experimental results show that the proposed model is effective in edge-preserving and staircase effect alleviatation in Poisson image denoising. Additionaly, compared with state-of-the-art variational models, the proposed model outperform other models in terms of PSNR and SSIM values.

2. THE PROPOSED MODEL AND ALGORITHM

2.1 The proposed model

In this paper, we focus on (3) and consider the following model for restoring Poissonian images:

$$\mathbf{X}^* = \arg\min_X \Big(\gamma_1 \int_{\mathcal{B}} \mathcal{G}(|\nabla \mathbf{X}|)dx + \gamma_2 \int_{\mathcal{B}} \mathcal{G}(|\nabla^\alpha \mathbf{X}|)dx + \beta \int_\Omega (\mathbf{X} - \mathbf{Y}\log \mathbf{X})dx, \Big), \tag{4}$$

where γ_1, γ_2 and β are positive parameters
$\mathcal{G}$ is a nonconvex and nonsmooth function.

In this work, we introduce a non-convex potential function $\mathcal{G}$ of the following stable form:

$$\mathcal{G}(|s|) = (|s| + \delta)^r, \tag{5}$$

where $r \in (0, 1)$ is scalar parameter, δ is the small positive, the operators $\nabla \mathbf{X}$ and $\nabla \mathbf{X}^\alpha$ are defined as follows (Aubert, 2006, Zhang et al. 2012):

$$\nabla_1 \mathbf{X}_{i,j} = \mathbf{X}_{i+1,j} - \mathbf{X}_{i,j},$$
$$\nabla_2 \mathbf{X}_{i,j} = \mathbf{X}_{i,j+1} - \mathbf{X}_{i,j},$$

$$\nabla \mathbf{X}_{i,j} = (\nabla_1 \mathbf{X}_{i,j}, \nabla_2 \mathbf{X}_{i,j}),$$
$$|\nabla \mathbf{X}_{i,j}| = \sqrt{(\nabla_1 \mathbf{X}_{i,j})^2 + (\nabla_2 \mathbf{X}_{i,j})^2}.$$

$$\nabla^\alpha \mathbf{X} = [\nabla_1^\alpha \mathbf{X}, \nabla_2^\alpha \mathbf{X}],$$
$$(\nabla_1^\alpha \mathbf{X})_{i,j} = \sum_{k=0}^{K-1} C_k^\alpha \mathbf{X}_{i-k,j},$$

$$(\nabla_2^\alpha \mathbf{X})_{i,j} = \sum_{k=0}^{K-1} C_k^\alpha \mathbf{X}_{i,j-k}.$$

From (4), (5), the proposed model has the discrete form as follows:

$$\min_X \Big(\gamma_1 (\|\nabla \mathbf{X}\|_1 + \delta)^r + \gamma_2 (\|\nabla^\alpha \mathbf{X}\|_1 + \delta)^r + \beta \langle \mathbf{1}, \mathbf{X} - \mathbf{Y}\log \mathbf{X}\rangle \Big), \tag{6}$$

By using the iteratively reweighted l_1 algorithm (Candes et al., 2008), we approximate the problem (6) as the following surrogate convex optimization problem

$$\min_{z,w} \Big(\gamma_1 q_1^{(k)} \|\nabla \mathbf{X}\|_1 + \gamma_2 q_2^{(k)} \|\nabla^\alpha \mathbf{X}\|_1 + \beta \langle 1, \mathbf{X} - \mathbf{Y}\log \mathbf{X}\rangle \Big), \tag{7}$$

where $q_1^{(k)} = \frac{r}{(\delta + \|\nabla \mathbf{X}^{(k)}\|_1)^{1-r}}$
$q_2^{(k)} = \frac{r}{(\delta + \|\nabla^\alpha \mathbf{X}^{(k)}\|_1)^{1-r}}$.

2.2 The proposed algorithm

Based on the splitting method (Huang et al., 2008, He et al., 2014, Goldstein, 2009), using three auxiliary variables and take effective replacements $\nabla \mathbf{X} \to \mathbf{Q}$, $\nabla^\alpha \mathbf{X} \to \mathbf{Z}$,$\mathbf{X} \to \mathbf{T}$, we convert (7) to the constrained problem as follows:

$$\min_{\vartheta,\omega,u} \Big(\gamma_1 q_1^{(k)} \|\mathbf{Q}\|_1 + \gamma_2 q_2^{(k)} \|\mathbf{Z}\|_1 + \beta \langle \mathbf{1}, \mathbf{X} - \mathbf{Y}\log \mathbf{X}\rangle \Big), \quad \text{s.t. } \mathbf{Q} = \nabla \mathbf{X}, \mathbf{Z} = \nabla^\alpha \mathbf{X}, \mathbf{T} = \mathbf{X}. \tag{8}$$

For solving (8), we determine the augmented Lagrangian function as follows:

$$\min_{\mathbf{Q},\mathbf{Z},\mathbf{T},\xi_1,\xi_2} = \Big(\gamma_1 q_1^{(k)} \|\mathbf{Q}\|_1 + \gamma_2 q_2^{(k)} \|\mathbf{Z}\|_1 + \beta \langle \mathbf{1}, \mathbf{T} - \mathbf{Y}\log \mathbf{T}\rangle - \langle \eta_1, \mathbf{Q} - \nabla \mathbf{X}\rangle + \frac{\omega}{2}\|\mathbf{Q} - \nabla \mathbf{X}\|_2^2 - \langle \eta_2, \mathbf{Z} - \nabla^\alpha \mathbf{X}\rangle + \frac{\omega}{2}\|\mathbf{Z} - \nabla^\alpha \mathbf{X}\|_2^2 - \langle \eta_3, \mathbf{T} - \mathbf{X}\rangle + \frac{\omega}{2}\|\mathbf{T} - \mathbf{X}\|_2^2 \Big), \tag{9}$$

where ω_1, ω_2 - positive parameters,
η_2 -Lagrangian multipliers

The minimization method to solve the problem (9) can be expressed as follows:

$$\begin{cases} \mathbf{X}^{(k+1)} = \arg\min_{\mathbf{X}} \Big(- \langle \eta_1^{(k)}, \mathbf{Q}^{(k)} - \nabla \mathbf{X} \rangle \\ + \frac{\omega}{2} \|\mathbf{Q}^{(k)} - \nabla \mathbf{X}\|_2^2 - \langle \eta_2^{(k)}, \mathbf{Z}^{(k)} - \nabla^\alpha \mathbf{X} \rangle \\ + \frac{\omega}{2} \|\mathbf{Z}^{(k)} - \nabla^\alpha \mathbf{X}\|_2^2 - \langle \eta_3^{(k)}, \mathbf{T}^{(k)} - \mathbf{X} \rangle \\ + \frac{\omega}{2} \|\mathbf{T}^{(k)} - \mathbf{X}\|_2^2 \Big), \\ \mathbf{Q}^{(k+1)} = \arg\min_{\mathbf{Q}} \Big(\gamma_1 q_1^{(k)} \|\mathbf{Q}\|_1 - \langle \eta_1^{(k)}, \mathbf{Q} - \nabla \mathbf{X}^{(k+1)} \rangle \\ + \frac{\omega}{2} \|\mathbf{Q} - \nabla \mathbf{X}^{(k+1)}\|_2^2 \Big), \\ \mathbf{Z}^{(k+1)} = \arg\min_{\mathbf{Z}} \Big(\gamma_2 q_2^{(k)} \|\mathbf{Z}\|_1 - \langle \eta_2^{(k)}, \mathbf{Z} - \nabla^\alpha \mathbf{X}^{(k+1)} \rangle \\ + \frac{\omega}{2} \|\mathbf{Z} - \nabla^\alpha \mathbf{X}^{(k+1)}\|_2^2 \Big), \\ \mathbf{T}^{(k+1)} = \arg\min_{\mathbf{T}} \Big(\beta \langle \mathbf{1}, \mathbf{T} - \mathbf{Y} \log \mathbf{T} \rangle - \langle \eta_3^{(k)}, \mathbf{T} - \nabla \mathbf{X}^{(k+1)} \rangle \\ + \frac{\omega}{2} \|\mathbf{T} - \nabla \mathbf{X}^{(k+1)}\|_2^2 \Big) \end{cases} \tag{10}$$

with update for $\eta_1^{(k+1)}, \eta_2^{(k+1)}$:

$$\begin{cases} \eta_1^{(k+1)} = \eta_1^{(k)} + \mu_1 (\nabla \mathbf{X}^{(k+1)} - \mathbf{Q}^{(k+1)}), \\ \eta_2^{(k+1)} = \eta_2^{(k)} + \mu_2 (\nabla^\alpha \mathbf{X}^{(k+1)} - \mathbf{Z}^{(k+1)}), \\ \eta_3^{(k+1)} = \eta_3^{(k)} + \mu_3 (\mathbf{X}^{(k+1)} - \mathbf{T}^{(k+1)}) \end{cases} \tag{11}$$

The $\mathbf{X}$ subproblem in (10) is given by:

$$\begin{aligned} \mathbf{X}^{(k+1)} = \arg\min_{\mathbf{X}} \Big(& - \langle \eta_1^{(k)}, \mathbf{Q}^{(k)} - \nabla \mathbf{X} \rangle \\ & + \frac{\omega}{2} \|\nabla \mathbf{X} - \mathbf{Q}^{(k)}\|_2^2 - \langle \eta_2^{(k)}, \mathbf{Z}^{(k)} - \nabla^\alpha \mathbf{X} \rangle \\ & + \frac{\omega}{2} \|\nabla^\alpha \mathbf{X} - \mathbf{Z}^{(k)}\|_2^2 - \langle \eta_3, \mathbf{T} - \mathbf{X} \rangle \\ & + \frac{\omega}{2} \|\mathbf{X} - \mathbf{T}\|_2^2 \Big) \end{aligned}$$

Thus, we get:

$$\begin{aligned} & \nabla^T \eta_1^{(k)} + \omega \nabla^T (\nabla \mathbf{X}^{(k+1)} - \mathbf{Q}^{(k)}) + (\nabla^\alpha)^T \eta_2^{(k)} \\ & + \omega (\nabla^\alpha)^T (\nabla^\alpha \mathbf{X}^{(k+1)} - \mathbf{Z}^{(k)}) \\ & + \eta_3 \mathbf{X} + \omega (\mathbf{X}^{(k+1)} - \mathbf{T}^{(k)}) = 0. \end{aligned}$$

We transform the above equation as:

$$\begin{aligned} & (\omega \nabla^T \nabla + \omega (\nabla^\alpha)^T \nabla^\alpha + \eta_3^{(k)}) \mathbf{X}^{(k+1)} \\ & = \nabla^T (\omega \mathbf{Q}^{(k)} - \eta_1^{(k)}) + (\nabla^\alpha)^T (\omega \mathbf{Z}^{(k)} - \eta_2^{(k)}) + \omega \mathbf{T}^{(k)} \end{aligned}$$

Based on (Wang, 2008), the subproblem $\mathbf{X}^{(k+1)}$ can be efficiently solved via fast Fourier transform as:

$$\mathbf{X}^{(k+1)} = \mathcal{F}^{-1} \Bigg(\frac{\mathcal{F}\Big(\mathbf{K}\Big)}{\Big(\omega \nabla^T (\nabla + \omega (\nabla^\alpha)^T \nabla^\alpha + \eta_3^{(k)} \Big)} \Bigg), \tag{12}$$

where $\mathcal{F}$ and $\mathcal{F}^{-1}$ are Fourier transform operators in the the forward and inverse directions

$$\mathbf{K} = \nabla^T (\omega \mathbf{Q}^{(k)} - \eta_1^{(k)}) + (\nabla^\alpha)^T (\omega \mathbf{Z}^{(k)} - \eta_2^{(k)}) + \omega \mathbf{T}^{(k)}$$

The subproblems $\mathbf{Q}$ and $\mathbf{Z}$ in in (10) are given by:

$$\begin{aligned} \mathbf{Q}^{(k+1)} = \arg\min_{\mathbf{Q}} \Big(& \gamma_1 q_1^{(k)} \|\mathbf{Q}\|_1 - \langle \eta_1^{(k)}, \mathbf{Q} - \nabla \mathbf{X}^{(k+1)} \rangle \\ & + \frac{\omega}{2} \|\mathbf{Q} - \nabla \mathbf{X}^{(k+1)}\|_2^2 \Big), \\ \mathbf{Z}^{(k+1)} = \arg\min_{\mathbf{Z}} \Big(& \gamma_2 q_2^{(k)} \|\mathbf{Z}\|_1 - \langle \eta_2^{(k)}, \mathbf{Z} - \nabla^\alpha \mathbf{X}^{(k+1)} \rangle \\ & + \frac{\omega}{2} \|\mathbf{Z} - \nabla^\alpha \mathbf{X}^{(k+1)}\|_2^2 \Big). \end{aligned}$$

For solving the $\mathbf{Q}$ and $\mathbf{Z}$ subproblems, we emply the shrinkage formula (Goldstein, 2009), as follows:

$$\mathbf{Q}^{(k+1)} = \text{Shrink}(\nabla \mathbf{X}^{(k+1)} + \frac{\eta_1^{(k)}}{\omega}, \frac{\gamma_1 q_1^{(k)}}{\omega}). \tag{13}$$

$$\mathbf{Z}^{(k+1)} = \text{Shrink}(\nabla^\alpha \mathbf{X}^{(k+1)} + \frac{\eta_2^{(k)}}{\omega}, \frac{\gamma_2 q_2^{(k)}}{\omega}). \tag{14}$$

where $\text{Shrink}(y, \varphi) = \frac{y}{|y|} \cdot \max(|y| - \varphi, 0)$.

The subproblem $\mathbf{T}^{(k+1)}$ in (10) is given by:

$$\begin{aligned} \mathbf{T}^{(k+1)} = \arg\min_{\mathbf{T}} \Big(& \beta \langle \mathbf{1}, \mathbf{T} - \mathbf{Y} \log \mathbf{T} \rangle - \langle \eta_3^{(k)}, \mathbf{T} - \nabla \mathbf{X}^{(k+1)} \rangle \\ & + \frac{\omega}{2} \|\mathbf{T} - \nabla \mathbf{X}^{(k+1)}\|_2^2 \Big) \end{aligned}$$

We have:

$$\beta (\mathbf{1} - \frac{\mathbf{Y}}{\mathbf{T}}) - \eta_3^{(k)} + \omega (\mathbf{T} - \nabla \mathbf{X}^{(k+1)})$$

Thus, we get:

$$\mathbf{a}_{(k)} (\mathbf{T}^{(k+1)})^2 + \mathbf{b}_{(k)} \mathbf{T}^{(k+1)} + \mathbf{c}_{(k)} = 0 \tag{15}$$

where
$$\begin{aligned} \mathbf{a}^{(k)} &= \omega \\ \mathbf{b}^{(k)} &= -(\omega \nabla \mathbf{X}^{(k+1)} + \eta_3^{(k)} - \beta)) \\ \mathbf{c}^{(k)} &= -\beta \mathbf{Y}. \end{aligned}$$

Easily, we realize that $\mathbf{T}^{(k+1)}$ is the positive solution of (15):

$$\mathbf{T}^{(k+1)} = \frac{-\mathbf{b}^{(k)} + \sqrt{(\mathbf{b}^{(k)})^2 - 4 \mathbf{a}^{(k)} \mathbf{c}^{(k)}}}{2 \mathbf{a}^{(k)}} \tag{16}$$

The proposed algorithm is presented in Algorithm (1).

Algorithm 1 Non-convex hybrid total variation for Poisson noise removal

Initialize: $\mathbf{X}^{(0)} = \mathbf{T}^{(0)} = \mathbf{Y}$, $\mathbf{Q}^{(0)} = \nabla\mathbf{X}^{(0)}$, $\mathbf{Z}^{(0)} = \nabla^{\alpha}\mathbf{X}^{(0)}$; $k = 1$
while $\left(\frac{\|\mathbf{X}^{(k)} - \mathbf{X}^{(k-1)}\|_2}{\|\mathbf{X}^{(k)}\|_2} > \epsilon\right)$ **do**
  Compute $\mathbf{X}^{(k+1)}$ according to (12)
  Compute $\mathbf{Q}^{(k+1)}$ according to (13)
  Compute $\mathbf{Z}^{(k+1)}$ according to (14)
  Compute $\mathbf{T}^{(k+1)}$according to (16)
  Compute $\mathbf{Z}^{(k+1)}$ by (14)
  Update η_1, η_2, η_3 according to (11)
  $k = k + 1$
end while
return $\mathbf{X}$

3. EXPERIMENTAL RESULTS

In this section we show some reconstruction results to illustrates the effectiveness of the proposed method. Image denoising quality is measured by the peak signal-to-noise ratio (PSNR) and the structure similarity index measure (SSIM) (Wang et al. 2004). We compare our denoising results with the results of HTVRM in (3). We tested algorithms with empirically determined parameters: $\epsilon = 0.0001$,$\alpha = 1.6$, $\gamma_1 = \gamma_2 = 0.5$, $\omega = 0.01$. All experiments were carried out on a system running Windows 10 64-bit with MATLAB version R2018b with Intel(R) Core(TM) i3-10110U CPU @ 2.10GHz, 2.50 GHz, 12GB RAM. Noisy observation is generated by Poisson noise using MATLAB command $poissrnd(\mathbf{X}/I_{max}) \times I_{max}$, where I_{max} is noise level.

Firstly, we show in Figure (1) the reconstruction results of compared methods with noisy level $I_{max} = 2$. The original image 'Knee'[1] (sized by 216×201 pixels) shown in Figure (1)a, while the noisy image is shown in (1)b. In second row (1)c,(1)d, we show the reconstructions via HTVRM and ours model respectively. In Figures (1)g–(1)h, we also enlarge some details of the images mentioned above.

Secondly, we show the reconstruction results for image 'Brain'[2] (sized by 230×265 pixels) and its zoomed details in Figures (2)a and (2)e. The noisy image with noise level $I_{max} = 4$ and its details are shown in (2)b, (2)f. The denoising results of compared methods are shown in (2)c, (2)d. The locally enlarged of these images are presented in (1)g,–(2)h.

In Tables (1), (2),we show the SSIM and PSNR measurements to quantitatively compare the results of the different methods.

Image	PSNR			SSIM		
	Noisy	HTVRM	Ours	Noisy	HTVRM	Ours
Brain	28.3151	30.0918	32.7677	0.7510	0.9094	0.9113
Knee	17.5244	25.4948	25.9863	0.6530	0.8166	0.8270

Table 1. PSNR and SSIM values for image denoising with $I_{max} = 2$

From the figures and tables we see that our proposed method gives better visual results than HTVRM. Furthermore, the results in Tables 1-2 show that the proposed method significantly improves the quality in terms of PSNR and SSIM quantification compared with the pre-existing method.

[1] Knee MRI scan,https://www.medserena.co.uk/mri-scans.
[2] Normal-brain-mri,https://radiopaedia.org/cases/normal-brain-mri-6.

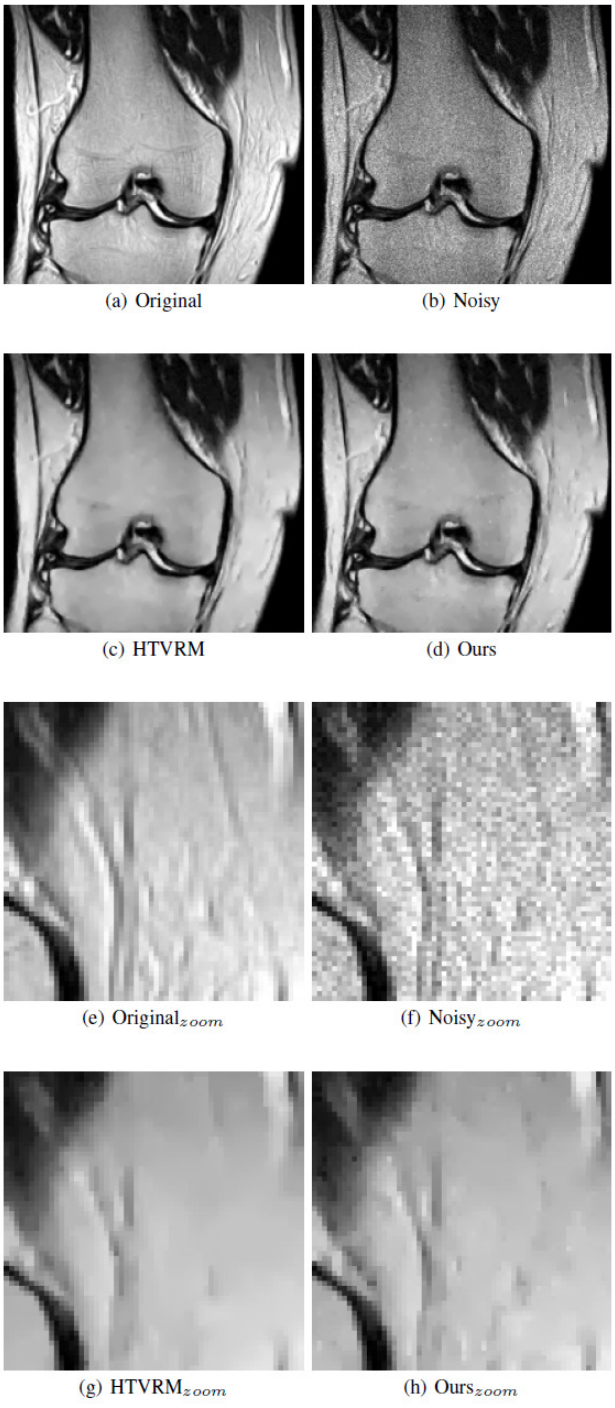

(a) Original (b) Noisy (c) HTVRM (d) Ours (e) Original$_{zoom}$ (f) Noisy$_{zoom}$ (g) HTVRM$_{zoom}$ (h) Ours$_{zoom}$

Figure 1. Image 'Knee'. Recovered results by compared methods with noise level $I_{max} = 2$

Image	PSNR			SSIM		
	Noisy	HTVRM	Ours	Noisy	HTVRM	Ours
Brain	25.4301	28.7532	30.1458	0.6464	0.8645	0.8750
Knee	14.2870	24.1209	25.3109	0.5443	0.7760	0.7830

Table 2. PSNR and SSIM values for image denoising with $I_{max} = 4$

4. CONCLUSION

In this paper, we have proposed a novel model based on the combination of non–convex first order total variation and non–

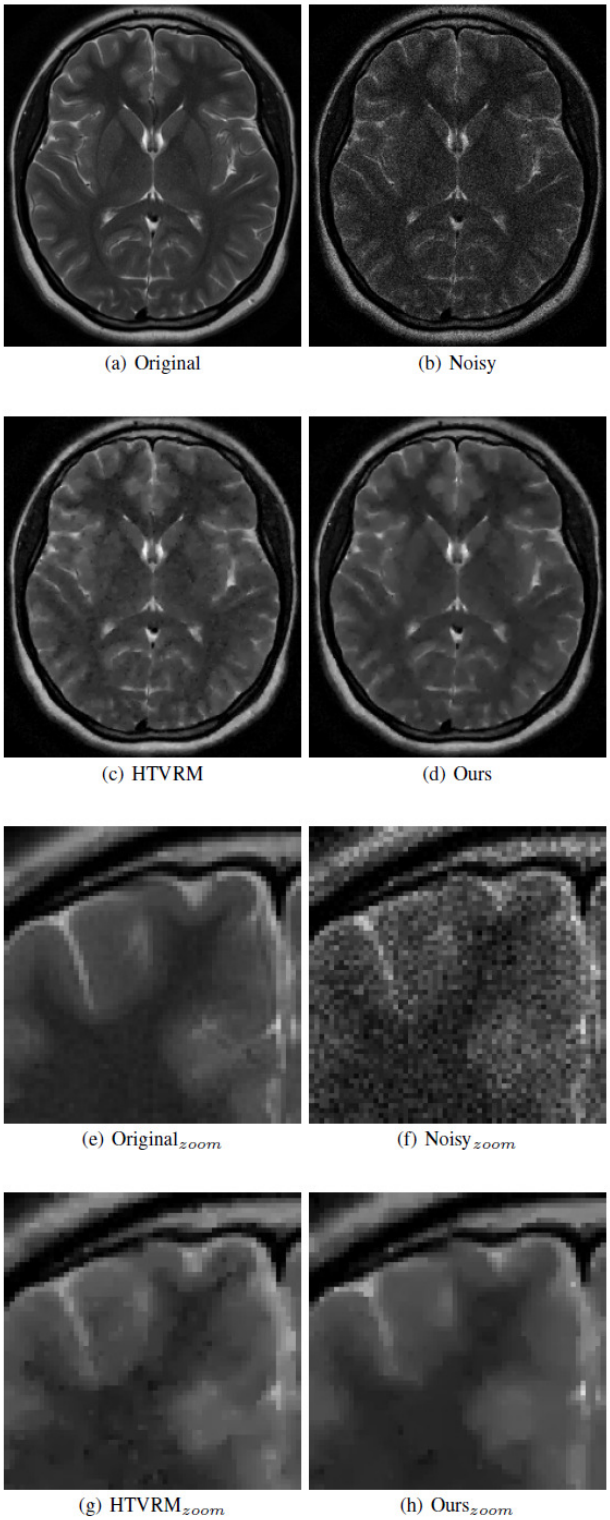

(a) Original (b) Noisy

(c) HTVRM (d) Ours

(e) Original$_{zoom}$ (f) Noisy$_{zoom}$

(g) HTVRM$_{zoom}$ (h) Ours$_{zoom}$

Figure 2. Image ‘Brain’. Recovered results by compared methods with noise level $I_{max} = 4$

convex fractional total variation. The proposed model allows for good image quality improvement with sharp and neat edges. We used the efficient alternating minimization algorithm to find optimal solution. Some experimental results have been given to prove the effectiveness of the proposed method.

5. ACKNOWLEDGEMENTS

This work is supported by The Murata Science Foundation and The University of Danang-University of Science and Technology, code number of Project **T2021-02-03MSF**

REFERENCES

Aubert G. , Kornprobst P., 2006. Mathematical Problems in Image Processing: partial differential equations and the calculus of variations. *Appl. Math. Sci.*. Springer–Verlag, New York, 147, 2 ed., 379 pages. doi.org/10.1007/978-0-387-44588-5.

Candes E.J., Wakin M.B., Boyd S.P., 2008. Enhancing sparsity by reweighted l_1 minimization. *J. Fourier Anal. Appl.*, 14, 877–905. doi.org/10.1007/s00041-008-9045-x

Chambolle, A., 2004. An algorithm for total variation minimization and applications. *J. Math. Imaging Vis.*, 26 (6), 89–97. doi.org/10.1023/B:JMIV.0000011325.36760.1e

Chowdhury M. R., Zhang J., Qin J., Lou Y., 2020. Poisson image denoising based on fractional-order total variation. *Inverse Probl. Imaging*, 14 (1), 77–96. doi.org/10.3934/ipi.2019064

Goldstein, T., Osher, S., 2009. The split Bregman method for L1-regularized problems. *SIAM J. Imaging Sci.*, 2 (2), 89-97. doi.org/10.1137/080725891.

Hasinoff S. W., 2014. Photon, poisson noise. *Computer vision*, 608-610. doi.org/10.1007/978-0-387-31439-6-482.

Huang, Y. M., Ng M. K., Wen Y. W., 2008. A fast total variation minimization method for image restoration. *Multiscale Model. Sim.*, 7 (2), 774-795. doi.org/10.1137/070703533.

He C., Hu C., Zhang W., Shi B., 2014. A Fast Adaptive Parameter Estimation for Total Variation Image Restoration. *IEEE Trans. Image Process.*, 23 (12), 4954-4967. doi.org/10.1109/TIP.2014.2360133.

Kayyar S.H., Jidesh P., 2018. Non-local total variation regularization approach for image restoration under a Poisson degradation. *J. Mod. Opt.* , 65 (19): 2231–2242. doi.org/10.1080/09500340.2018.1506058

Le T. , Chartrand R., Asaki T., 2007. A variational approach to constructing images corrupted by Poisson noise. *J. Math. Imaging Vis.* 27 (2007), 257-263. doi.org/10.1007/s10851-007-0652-y

Lian W., Liu X., 2023. Non-convex fractional-order TV model for impulse noise removal. *J. Comput. Appl. Math.*, 417 (1), 114615. doi.org/10.1016/j.cam.2022.114615

Liu J. et al., 2013. High-order total variation-based multiplicative noise removal with spatially adapted parameter selection. *J. Opt. Soc. Am. A*, 30 (10), 1956-1966. doi.org/10.1364/JOSAA.30.001956.

Ma M., Zhang J., Deng C., Liu Z., Wang Y., 2020. Adaptive Image Restoration via a Relaxed Regularization of MeanCurvature. *Math. Probl. Eng.*, 2020:416907, 1-11. doi.org/10.1155/2020/3416907

Nikolova M., Ng M.K., Tam C.P., 2010. Fast Non-convex nonsmooth minimization methods for image restoration and reconstruction. *IEEE Trans. Image Process.*, 19 (12), 3073–3088. doi.org/10.1109/TIP.2010.2052275.

Pham C.T et al., 2023. An adaptive image restoration algorithm based on hybrid total variation regularization. *Turk. J. Elec. Eng. & Comp. Sci.*, 31 (1), 1–16. doi.org/10.55730/1300-0632.3968.

Pham C.T, Tran T.T.T., 2021. An algorithm for hybrid regularizers based image restoration with Poisson noise. *Kybernetika*, 57 (3), 446-473. doi.org/10.14736/kyb-2021-3-0446.

Pham C. T. et al., 2021 Combined total variation of first and fractional orders for Poisson noise removal in digital images. *Inf. Control Sys.*, 5, pp. 10–19. doi:10.31799/1684-8853-2021-5-10-19

Tang L., Ren Y., Fang Z., He C., 2019. A generalized hybrid nonconvex variational regularization model for staircase reduction in image restoration. *Neurocomputing*, 359 (24), 15–31. doi.org/10.1016/j.neucom.2019.05.073

Tran T.T.T., Pham C.T., 2021. A hybrid regularizers approach based model for restoring image corrupted by Poisson noise. *Comput. Res. Model*, 13 (5), 965–978. doi.org/10.20537/2076-7633-2021-13-5-965-978

Wang Y., Yang J., Yin W., Zhang Y., 2008. A New Alternating Minimization Algorithm for Total Variation Image Reconstruction. *SIAM Journal on Imaging Sciences.*, 1 (3), 248-272. doi.org/10.1137/08072426

Wang, Z., Bovik, A.C., Sheikh, H.R., Simoncelli, E.P., 2004. Image quality assessment: from error visibility to structural similarity. *IEEE Trans. Image Process.*, 13(4), 600–612. doi.org/10.1109/TIP.2003.819861.

Zhang J., Wei Z., Xiao L., 2012. Adaptive fractional-order multi-scale method for image denoising. *J. Math. Imaging Vision.*, 43, 39-49. doi.org/10.1007/s10851-011-0285-z